Implications of RNG140 (caprin2)-mediated translational regulation in eye lens differentiation

Received for publication, January 18, 2020, and in revised form, August 7, 2020 Published, Papers in Press, August 23, 2020, DOI 10.1074/jbc.RA120.012715

Kaori Nakazawa[1,2], **Yuichi Shichino**[3], **Shintaro Iwasaki**[3,4], **and Nobuyuki Shiina**[1,2,5,*]

From the [1]*Laboratory of Neuronal Cell Biology, National Institute for Basic Biology, Okazaki, Aichi, Japan, the* [2]*Department of Basic Biology, SOKENDAI (Graduate University for Advanced Studies), Okazaki, Aichi, Japan, the* [3]*RNA Systems Biochemistry Laboratory, RIKEN Cluster for Pioneering Research, Saitama, Japan, the* [4]*Department of Computational Biology and Medical Sciences, Graduate School of Frontier Sciences, University of Tokyo, Chiba, Japan, and the* [5]*Exploratory Research Center on Life and Living Systems (ExCELLS), Okazaki, Aichi, Japan*

Edited by Ronald C. Wek

Regulation of gene expression at the translational level is key to determining cell fate and function. An RNA-binding protein, RNG140 (caprin2), plays a role in eye lens differentiation and has been reported to function in translational regulation. However, the mechanism and its role in eyes has remained unclear. Here, we show that RNG140 binds to the translation initiation factor eukaryotic initiation factor 3 (eIF3) and suppresses translation through mechanisms involving suppression of eIF3-dependent translation initiation. Comprehensive ribosome profiling revealed that overexpression of RNG140 in cultured Chinese hamster ovary cells reduces translation of long mRNAs, including those associated with cell proliferation. RNG140-mediated translational regulation also operates in the mouse eye, where RNG140 knockout increased the translation of long mRNAs. mRNAs involved in lens differentiation, such as crystallin mRNAs, are short and can escape translational inhibition by RNG140 and be translated in differentiating lenses. Thus, this study provides insights into the mechanistic basis of lens cell transition from proliferation to differentiation via RNG140-mediated translational regulation.

Gene expression is an essential process in development, cell differentiation, and other diverse processes in organisms and is regulated in multiple steps. Although transcriptional control has received much attention, post-transcriptional steps such as mRNA splicing, polyadenylation, stabilization, transport, and translation are also important layers of gene expression control (1–5). Apparently, RNA-binding proteins play a central role in the post-transcriptional gene regulation (6, 7).

RNA granule protein 140 (RNG140, also known as caprin2) is such an RNA-binding protein that regulates cell differentiation and various functional processes. For example, RNG140 functions in embryonic development through facilitating canonical Wnt/β-catenin signaling (8). In erythroid cells, RNG140 expression increases during the cells' shift from a proliferative state to a differentiated state (9). Indeed, RNG140 expression negatively correlates with cell growth in Chinese hamster ovary (CHO) cells (9), confirming its role in inhibiting cell proliferation. In addition to cell differentiation, RNG140 is highly expressed in the brain and is involved in processes such as the formation and maintenance of dendrites and synapses (10) and the osmotic stress response in the hypothalamus (11).

Because RNG140 has two RNA-binding coiled-coil and RGG box domains (10), its function may be attributed to the RNA-binding activity. For example, RNG140 has been reported to bind to arginine vasopressin (*AVP*) mRNA and stabilize the mRNA by increasing poly(A) tail length in response to osmotic stress in the hypothalamus (11). Alternatively, RNG140 may function as a hub of protein interaction through a C-terminal C1q domain, which often undergoes trimerization (12): it interacts with low-density lipoprotein receptor–related protein 5/6 (LRP5/6) and Cpn1027 via the C1q domain and enhances phosphorylation of LRP5/6 to mediate Wnt/β-catenin signaling (13, 14).

Like many other developmental processes, gene expression during the eye lens development is highly controlled. In this context, transcriptional regulation has been studied well: transcription factors such as Pax6, Six3, and Sox2 drive the progression of lens development, and those including Pax6 directly regulate the transcription of the lens-specific proteins such as crystallins (15, 16). In contrast, understanding of the post-transcriptional control during lens development is still limited (15, 17) except for the involvement of RNA-binding proteins as follows: Tudor domain–containing 7 (TDRD7) deficiency in mice reduced the level of target transcripts, such as the heat shock protein *Hspb1* mRNA and the crystallin *Crybb3* mRNA, and caused cataract and glaucoma (18). In zebrafish, the loss of the eukaryotic translation initiation factor *eif3ha* gene reduced translation of crystallin *crygm2d7* mRNA and caused brain and eye development defects (19). As a post-transcriptional gene regulator, RNG140 is one such example in lens development. During lens differentiation, RNG140 expression is increased by fibroblast growth factor (20, 21). Indeed, RNG140 conditional knockout in mice caused lens compaction defects and features of Peters anomaly (20).

RNG140 has been shown to inhibit translation in rabbit reticulocyte lysates (10). However, it is not known how RNG140 blocks translation and how the translational regulation is relevant to the *in vivo* function of RNG140, such as lens differentiation. Here, we show that RNG140 represses translation in an mRNA-selective manner. Protein interaction and internal ribosome entry site (IRES)-based reporter assays suggested that

This article contains supporting information.

* For correspondence: Nobuyuki Shiina, nshiina@nibb.ac.jp.

RNG140 blocks eIF3 in translation initiation. Moreover, genome-wide ribosome profiling in RNG140-overexpressing CHO cells and RNG140 knockout mouse eyes indicated that RNG140-mediated translational repression is biased toward long mRNAs. Thus, short mRNAs, including crystallin mRNAs, which are important for lens differentiation, escape RNG140-mediated translational repression. Our study suggested that RNG140 shifts the translational balance of gene expression from a proliferative state to a differentiated state.

Results

RNG140 increases inactive ribosomes and reduces translation in CHO cells

We examined the effect of RNG140 on translation in cells. To this end, we set out to perform ribopuromycilation of nascent polypeptides in cells that expressed RNG140-GFP (Fig. 1, *A–D*). First, RNG140-GFP or GFP was transiently expressed in CHO cells, and puromycin-staining intensity of those cells was compared with that of nearby untransfected control cells. RNG140-GFP expression, but not GFP expression, significantly reduced puromycin staining compared with control cells, especially at higher doses, suggesting that global translation was suppressed by RNG140 expression (Fig. 1, *A* and *B*). This effect of RNG140-GFP expression on translation was independent of cell type, as essentially the same results were obtained with another cell line, SRA 01/04, a human lens epithelial cell line (Fig. 1, *C* and *D*).

We examined whether native RNG140 exerts translational repression independent of the GFP tag. Transient overexpression of RNG140 in CHO cells was confirmed by Western blotting with anti-RNG140 antibody (Fig. 1*E*). In the ribopuromycilation assay, RNG140-transfected cells were distinguished from untransfected cells by co-transfection of mRFP1. It was estimated that about 96% of the mRFP1-positive cells expressed exogenous RNG140, judging from experiments in which CHO cells co-transfected with two plasmids encoding GFP and mRFP1 showed co-expression of the proteins in 96.4 ± 6.9% of mRFP1-positive cells. Puromycin staining was significantly reduced in mRFP1-positive cells co-transfected with RNG140, but not in mRFP1-positive cells not transfected with RNG140, compared with nearby untransfected cells (Fig. 1, *F* and *G*). These results validated that RNG140 represses translation.

Next, we generated CHO cell clones that stably expressed RNG140-GFP. The expression levels of RNG140-GFP were about twice that of endogenous RNG140 in mouse eyes (Fig. 1*H*). However, RNG140-GFP did not form RNA granules in those clones, suggesting that RNG140-GFP levels were below the critical concentration for granule formation and not toxic levels (10). In addition, because expression of RNG140 in the eye is restricted to the lens region, the expression level of RNG140 in the lens is higher than the average expression level in the whole eye and may be comparable with the RNG140-GFP levels in the CHO clones.

To compare puromycin staining between cells expressing RNG140-GFP and GFP in the same specimen, the CHO cell clones were co-cultured on the same coverslips (Fig. 1, *I* and *J*). RNG140-GFP– and GFP–expressing cells were distinguishable by predominant localization of the GFP signal in the cytoplasm and nucleus, respectively. These different distribution patterns may be due to the following reasons. GFP was distributed in both the cytoplasm and nucleus of living cells; however, in the ribopuromycilation assay, cytoplasmic GFP, but not nuclear GFP, was effluxed from the cells because the cell membrane, but not the nuclear membrane, was permeabilized with digitonin before fixation. As a result, GFP localization appeared to be prominent in the nucleus. In contrast, RNG140-GFP was localized only to the cytoplasm and may be anchored to certain scaffolds in the cytoplasm, which may be the reason why the RNG140-GFP signal remained in the cytoplasm after digitonin treatment. Cells stably expressing RNG140-GFP significantly reduced the staining for puromycin compared with GFP, indicating that global translation was suppressed by RNG140 expression (Fig. 1, *I* and *J*).

These results were further complemented by quantitative analysis of the stable clones by Western blotting for puromycin (SUnSET method). Total puromycin incorporation into nascent polypeptides was lower in RNG140-GFP–expressing cells than in GFP-expressing cells, confirming global translational suppression by RNG140 expression (Fig. 1, *K* and *L*).

We further analyzed the effect of RNG140 expression on the polysome profile using sucrose density gradient centrifugation (Fig. 2, *A–D*). After centrifugation, the sample was fractionated into 22 fractions, the amount of RNA in each fraction was measured at an absorbance of 254 nm, and the relative amount of RNA in each fraction was calculated. This analysis detected a fraction with a slightly higher RNA peak in RNG140-GFP-expressing cells than in GFP-expressing cells (Fig. 2*A*, *fraction 7*, *arrowhead*). EDTA treatment is known to release 80S ribosomes from polysomes and increase the amount of 60S and 40S subunits. This treatment reduced the relative RNA amount in fractions 11–19 and increased the amount in fractions 3–5, suggesting that these fractions corresponded to polysomes and 40S and 60S subunits, respectively (Fig. 2*B*). These positions of polysomes, 40S, and 60S were confirmed by the sedimentation profile of 18S and 28S rRNA analyzed with and without EDTA (Fig. 2*D*). Therefore, we reasoned that the fraction 7, sedimented between the polysomes and 40S and 60S subunits, corresponded to the 80S peak. Although the difference in the polysome profile between the two groups was modest in the presence of cycloheximide (Fig. 2*A*), removing cycloheximide from the buffers, which increases ribosome drop-off from mRNA, enhanced the difference between the two groups: the 80S peak did not increase in GFP-expressing cells but did increase in RNG140-GFP–expressing cells (Fig. 2*C*, *arrowhead*). This suggested that ribosomes formed 80S after drop-off from mRNA and/or ribosomes did not initially bind to mRNA at the 80S peak in RNG140-GFP–expressing cells. Thus, RNG140 appeared to increase 80S ribosomes that are not engaged on mRNAs.

To have more evidence of translational repression, we probed eukaryotic elongation factor 2 (eEF2) on ribosomes, which is a hallmark of inactive 80S (22). Ribosome pellets collected through a sucrose cushion showed that RNG140-GFP increased the recovery of eEF2, whereas an equivalent amount of ribosomes (S6 small subunit protein) and initiation factor

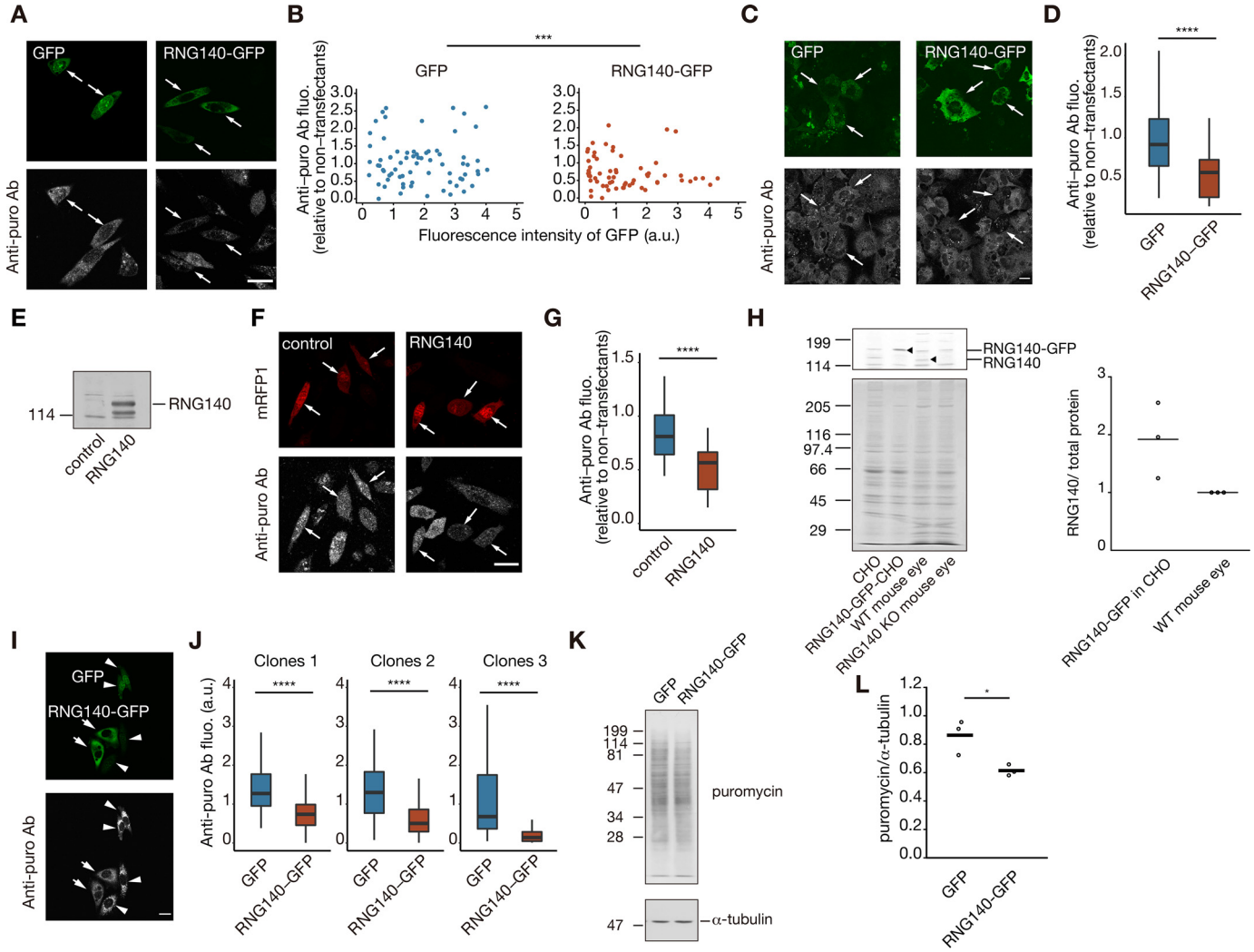

Figure 1. Decreased translation in RNG140-GFP–expressing cells. *A*, CHO cells transiently transfected with GFP and RNG140-GFP were analyzed by a ribopuromycilation assay to measure translation in cells. *Ab*, antibody. *Arrows*, transfected cells. *Scale bars* in *A*, *C*, *F*, and *I*, 20 μm. *B*, relationship between fluorescence intensities of GFP and puromycin staining in cells in *A*. Puromycin-staining intensity of the transfected cells was compared with that of nearby untransfected control cells. GFP-expressing cells, $n = 72$; RNG140-GFP-expressing cells, $n = 63$; ***, $p = 0.00123$, main effect in analysis of covariance. *C*, SRA 01/04 cells transiently transfected with GFP and RNG140-GFP were analyzed as in *A*. *D*, quantification of puromycin staining in cells in *C*. GFP-expressing cells, $n = 27$; RNG140-GFP–expressing cells, $n = 39$; ****, $p = 0.000117$, *t* test. *E*, Western blotting of CHO cells transiently transfected with RNG140 untagged with GFP with anti-RNG140 antibody. *F*, cells in *E* were analyzed by a ribopuromycilation assay. *Arrows*, transfected cells as judged by mRFP1 co-transfection. *G*, quantification of puromycin staining in cells in *F*. Control cells, $n = 17$; RNG140-expressing cells, $n = 18$; ****, $p = 0.000680$, *t* test. *H*, CHO cells stably transfected with RNG140-GFP (clone 1) and mouse eyes were analyzed by Western blotting with anti-RNG140 antibody (*top*) and Coomassie Brilliant Blue staining (*bottom*). RNG140-GFP expression levels, normalized to total protein levels, were compared with endogenous RNG140 expression levels in WT mouse eyes (*right*). *Arrowheads*, RNG140-GFP and endogenous RNG140 that was not detected in RNG140 knockout mice. See Fig. 5 for RNG140 knockout mice. *I*, CHO stable transfectants were analyzed by a ribopuromycilation assay. *Arrows* and *arrowheads*, RNG140-GFP– and GFP–expressing cells, respectively. *J*, quantification of puromycin staining in cells in *I*. Results of three clones are shown. The numbers of cells expressing GFP and RNG140-GFP are 132 and 101 (clones 1), 38 and 39 (clones 2), and 47 and 41 (clones 3), respectively. ****, $p < 2.2e{-}16$ (clones 1), $p = 1.23e{-}5$ (clones 2), and $p = 3.78e{-}8$ (clones 3), *t* test. *K*, the stable clones (clones 1) were analyzed by Western blotting for puromycin incorporation into nascent polypeptides and for α-tubulin as a control. *L*, quantification of puromycin staining normalized to α-tubulin in *K*. $n = 3$; *, $p = 0.0293$, *t* test.

eIF3b was found, compared with GFP expression (Fig. 2*E*). These results further supported the notion that RNG140 increases free 80S ribosomes, which was relevant to global translational suppression by RNG140.

RNG140 binds with eIF3 and reduces eIF3-dependent translation

Given that RNG140 was also found in sucrose cushion pellet (Fig. 2*E*), we reasoned that RNG140 associates with ribosome proteins or translation initiation factors that are typically co-sedimented in the sucrose cushion. To identify RNG140-associated proteins, we performed immunoprecipitation with RNG140-GFP followed by MS. We found that about 150 proteins specifically co-immunoprecipitated with RNG140-GFP but not with GFP (Fig. 3*A* and Table S1). Gene ontology (GO) enrichment analysis revealed that eIF3 subunit proteins and small ribosomal subunit proteins were significantly enriched in the RNG140-associated complex (Fig. 3*B*).

Western blotting of the immunoprecipitates confirmed the association of RNG140 with eIF3 subunits and S6 ribosomal

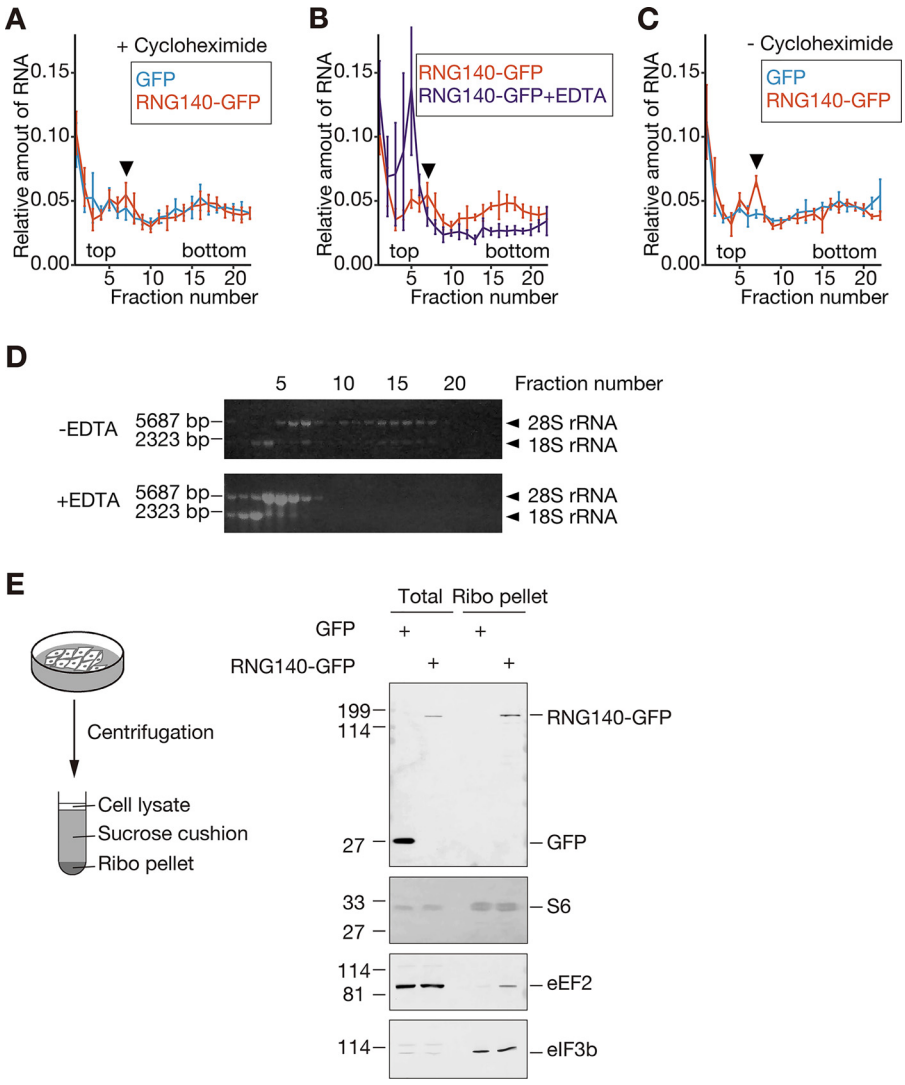

Figure 2. Increased inactive ribosomes in RNG140-GFP–expressing cells. *A–C*, polysome profiles of CHO cells stably expressing GFP and RNG140-GFP analyzed by sucrose density gradient centrifugation. Shown are the relative amount of RNA in each fraction, normalized to the total amount of RNA in the 22 fractions. Data are represented as the mean ± S.D. *A*, polysome profiling with cycloheximide. *B*, polysome profiling without or with EDTA, which dissociates polysome-associated ribosomes into 60S and 40S subunits. *C*, cycloheximide-free polysome profiling that allows ribosomes to drop-off from mRNA. *Arrowheads* denote the peak of 80S ribosomes. *D*, representative agarose gel electrophoresis of RNA from fractions of GFP-expressing cell lysates treated with and without EDTA. *E*, whole-cell lysates (*total*) and ribosome pellets (*Ribo pellet*) from the CHO stable transfectants were immunoblotted with anti-GFP, anti-ribosomal S6, anti-eEF2, and anti-eIF3b antibodies. Ribosome pellet was prepared in the presence of cycloheximide through a sucrose cushion.

protein (Fig. 3, *C* and *E*). This association of RNG140 with eIF3 was independent of cell type, as reproduced in SRA 01/04 cells (Fig. 3*D*). Attempts at reciprocal immunoprecipitation using anti-eIF3b antibody were inconclusive. The reason for this was unknown, but it could be that RNG140 interaction precluded the antibody binding to eIF3b. Treatment of the RNG140 immunoprecipitates with RNase A sustained the association of eIF3b with RNG140 (Fig. 3*E*), showing RNA-independent interaction of these proteins. We observed that S6 ribosomal protein was lost from the RNG140-associated complex by RNase A treatment, which may be because ribosomal small subunits bound to RNG140 through mRNA, or alternatively ribosome integrity was lost by RNase A treatment. These results, together with the MS data, suggested that RNG140 forms a complex with eIF3 through protein–protein interactions.

The RNG140-eIF3 interaction led us to hypothesize that RNG140 inhibits the function of eIF3 for translational repression. To examine this, we monitored translation driven by eIF3-dependent and -independent mechanisms using reporters. In the designed reporters, three different sequences were placed in front of *Renilla* luciferase: endogenous 5′-UTR (*EIF2S3*), hepatitis C virus (HCV) IRES, and cricket paralysis virus (CrPV) IRES. The former two require eIF3 and eIF2 for translation, whereas the last one does not (23). In CHO cells, RNG140 expression did not affect CrPV IRES–mediated translation but repressed HCV IRES– and *EIF2S3* 5′-UTR–mediated translation (Fig. 3*F*). These results further supported the idea that RNG140 represses eIF3-dependent translation but not eIF3-independent translation, although they did not rule out the possibilities that RNG140 also represses eIF2-dependent translation and other translation mechanisms.

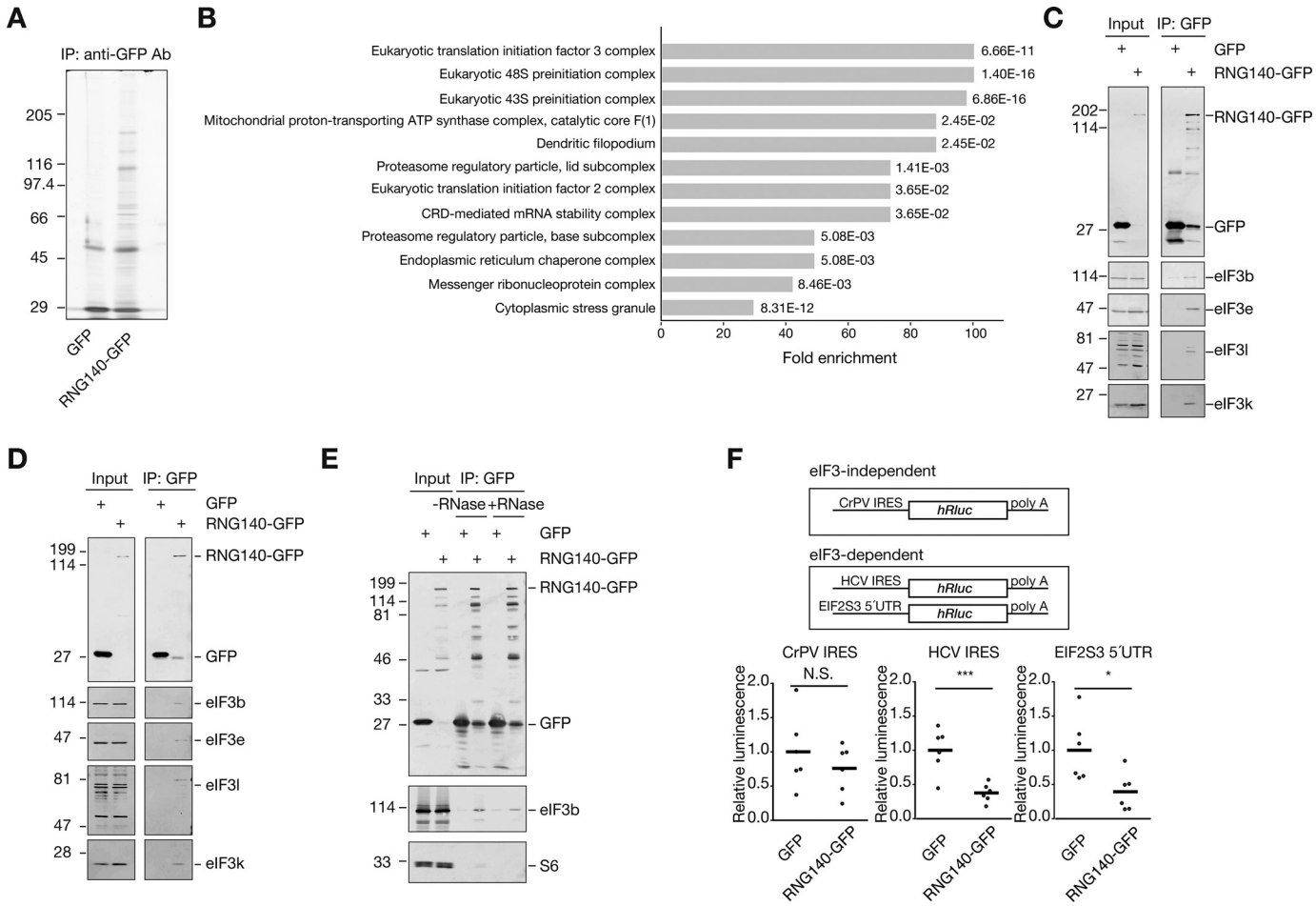

Figure 3. RNG140 binds with eIF3 and reduces eIF3-dependent translation in CHO cells. *A*, immunoprecipitates (*IP*) with anti-GFP antibody (*Ab*) from CHO cells stably expressing GFP and RNG140-GFP were silver-stained after SDS-PAGE. *B*, gene ontology enrichment analysis of RNG140-associated proteins. eIF3 subunit proteins and small ribosomal subunit proteins were included in the top categories. *C*, input extracts and the immunoprecipitates from the CHO stable transfectants were immunoblotted with anti-GFP and anti-eIF3 subunit antibodies. *D*, experiments similar to *C* using SRA 01/04 transient transfectants. *E*, immunoprecipitation from the CHO stable transfectants in the presence or absence of RNase A. Immunoprecipitates were immunoblotted with anti-GFP, anti-eIF3b, and anti-ribosomal S6 antibodies. *F*, CHO cells stably expressing GFP and RNG140-GFP were transfected with a reporter construct in which luciferase is translated under the control of CrPV IRES (*left*), HCV IRES (*middle*), or EIF2S3 5′-UTR (*right*) and evaluated for luciferase activity. $n = 6$; ***, $p = 0.0015$; *, $p = 0.0209$; *N.S.*, $p = 0.373$, *t* test.

RNG140 reduces translation of a set of mRNAs in CHO cells

Because translation of endogenous mRNAs is thought to be driven by eIF3, we wondered which mRNAs are affected by RNG140 in cells. Here, we performed ribosome profiling (24–26) upon RNG140 overexpression in CHO cells (Table S2). We identified 1,113 transcripts decreased in translation efficiency, which is calculated by over- or underrepresentation of footprint reads over RNA-Seq reads, by RNG140-GFP expression (Fig. 4 (*A* and *B*) and Table S3). We designated these as "more likely target transcripts" (more-T). Ribosome profiling also identified 860 transcripts with increased translation efficiency (Fig. 4 (*A* and *B*) and Table S4). We designated them as "less likely target transcripts" (less-T).

To validate the effect of RNG140 expression on translation efficiency, we analyzed the expression levels of proteins encoded by representative transcripts in the more-T (*Atr* and *Pola1*) and less-T (*Rps18* and *Fbl*) groups by Western blotting. RNG140-GFP reduced the expression levels of ATR and POLA but not RPS18 or FBL in CHO cells (Fig. 4*C*). These results confirmed that RNG140 reduces the translation efficiency of more-T group transcripts.

RNG140 and its paralog RNG105 (caprin1) share the conserved N-terminal basic helix domains, which have low sequence specificity for binding to mRNAs. This low-specificity binding is essential for the ability of RNG140 to suppress translation *in vitro* (10, 27). Given this property, RNG140 could preferentially bind to longer mRNAs that may provide multiple binding sites for RNG140. This idea has been suggested for mRNAs in stress granules, where mRNA length correlates with targeting to the granules (28). This idea led us to compare the length and the number of exons between the more-T and less-T groups. The length of the 5′-UTR, 3′-UTR, and coding sequence (CDS), and the number of coding exons of transcripts were compared between the top 100 in the more-T and less-T groups (Fig. 4*D* and Tables S3 and S4). As a result, the length of CDS and the number of coding exons for the more-T group were markedly larger than those of the less-T group (Fig. 4*D*), suggesting that RNG140 preferentially targets transcripts with longer CDS and more coding exons to repress translation.

Next, to identify the biological categories in which the more-T and less-T groups are involved, GO enrichment analysis was conducted (Fig. 4*E* and Tables S5 and S6). Major categories with

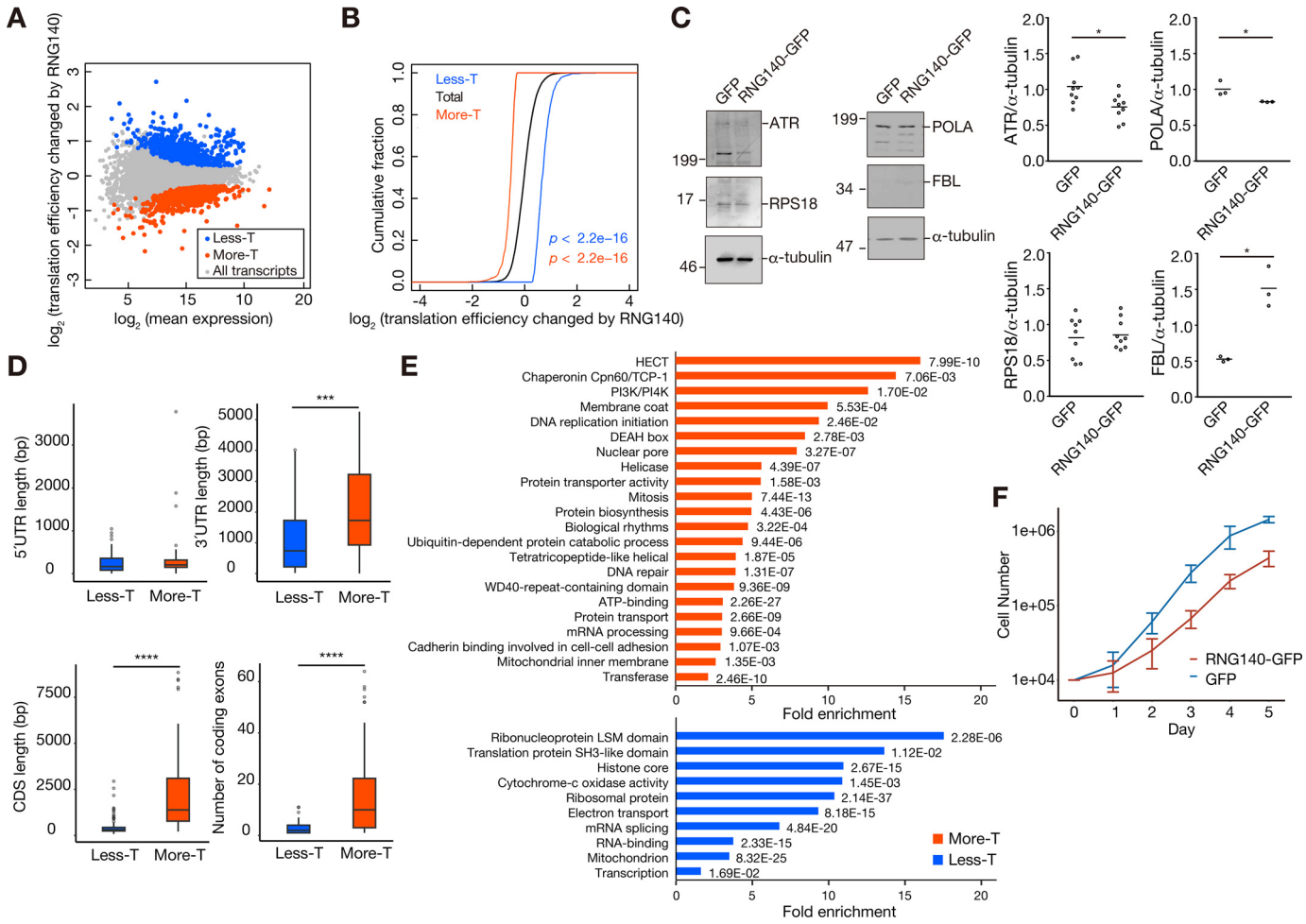

Figure 4. RNG140 reduces translation of mRNAs that are long and associated with proliferation in CHO cells. *A*, an MA plot of mean transcript expression and the -fold change in translation efficiency of the transcripts by RNG140 stable expression in CHO cells. Transcripts with decreased and increased translation efficiency by RNG140 expression (more-T and less-T, respectively) were identified statistically from two independent experiments with ribosome profiling and RNA-Seq analysis. *B*, cumulative distribution fraction plots showing changes in translation efficiency of total transcripts and transcripts in the more-T and less-T groups by RNG140 expression. Significance is calculated by Mann–Whitney *U* test. *C*, the stable clones (clones 1) were analyzed by Western blotting for proteins translated from more-T (*Atr* and *Pola1*) and less-T (*Rps18* and *Fbl*). Their band intensities were normalized to those of α-tubulin (*right panels*). ATR, $n = 9$ (*, $p = 0.0149$); POLA, $n = 3$ (*, $p = 0.0444$); RPS18, $n = 9$ ($p = 0.676$); FBL, $n = 3$ (*, $p = 0.0252$); *t* test. *D*, the top 100 transcripts in the more-T and less-T groups were analyzed for 5′-UTR length, 3′-UTR length, CDS length, and the number of coding exons. ***, $p = 0.00237$ for 3′-UTR length; ****, $p = 1.02e{-}12$ (for CDS length) and $3.85e{-}12$ (for the number of coding exons); *t* test. *E*, gene ontology enrichment analysis of the more-T (*red*) and less-T (*blue*) groups. *F*, cell proliferation measurement of CHO cells stably expressing GFP and RNG140-GFP. Data are represented as the mean ± S.D.

high -fold enrichment in the more-T group were "HECT" (a domain found in ubiquitin ligases), "chaperonin Cpn60/TCP-1," "PI3K/PI4K" (phosphoinositide 3/4-kinase), "membrane coat," "DNA replication initiation," etc. (Fig. 4*E* and Table S5). These categories contained a number of factors involved in cell proliferation (*e.g.* ubiquitin ligases (UBE3A (29), UBE3C (30), and NEDD4 (31)), PI3K (32), PI3K-related kinases such as TRRAP (33), DNA replication initiators, and mitotic regulatory proteins).

These gene categories were reminiscent of the function of RNG140 in inhibiting cell proliferation (9). Therefore, we tested whether overexpression of RNG140 affected the proliferation of CHO cells. Compared with GFP, RNG140-GFP expression decreased the rate of cell growth (Fig. 4*F*). Taking ribosome profiling data together, the results suggested that RNG140-mediated translational repression of cell proliferation–associated mRNAs slows the cell growth.

Generation of RNG140 knockout mice

To investigate whether the RNG140-mediated translational regulation operates *in vivo*, we generated RNG140 knockout mice by CRISPR/Cas9-mediated genome editing. We first obtained a heterozygous mutant, which had a 5-bp deletion in exon 6 of the *Rng140* genome (Fig. 5*A*). This deletion caused a frameshift in the *Rng140* ORF and generated a downstream premature stop codon in exon 7 (Fig. 5*A*). If the truncated protein were synthesized, it would contain the N-terminal basic helix domain that binds to mRNA and inhibits translation *in vitro* (10). However, the premature stop codon in the seventh exon of a total of 19 exons was expected to cause nonsense-mediated decay of mRNA, resulting in much less expression of the truncated form. This was indeed the case, as analyzed below. By crossing heterozygous ($Rng140^{+/-}$) mice, we obtained RNG140 knockout ($Rng140^{-/-}$) mice (Fig. 5, *B* and *C*), which

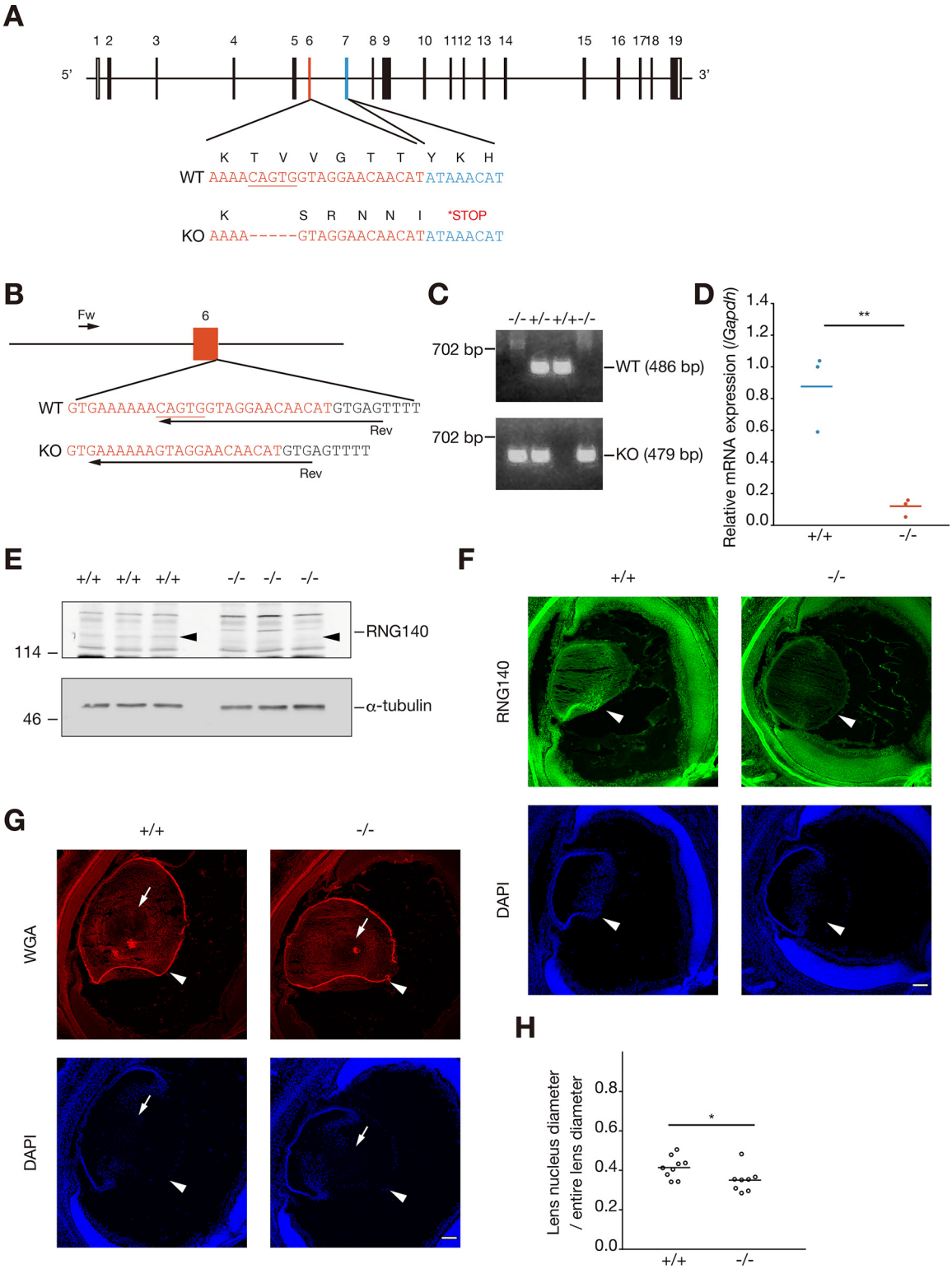

Figure 5. Generation of RNG140 knockout mice. *A*, gene structure of the *Rng140* genome. Nucleotide and amino acid sequences of WT (*top*) and *Rng140* knockout (*bottom*) alleles are shown. The first lysine (*K*) corresponds to the 210th amino acid of total 1,031 amino acids of RNG140. A 5-bp deletion in the exon 6 sequence (*red*) caused a frameshift and generated a downstream premature stop codon in the exon 7 sequence (*blue*). *B*, the genomic region around exon 6 and nucleotide sequences of WT and *Rng140* knockout alleles. *Arrows*, primer sets for PCR genotyping in *C*. *C*, PCR genotyping of the indicated genotypes. *D*, qRT-PCR analysis of *Rng140* mRNA in P0.5 $Rng140^{+/+}$ and $Rng140^{-/-}$ mouse eyes using exon 2–4 primers. *Rng140* mRNA expression was normalized by that of *Gapdh* mRNA. $n = 3$; **, $p = 0.00667$; *t* test. *E*, Western blotting of eyes from P0.5 $Rng140^{+/+}$ and $Rng140^{-/-}$ mice for RNG140 and α-tubulin as a control. *Arrowheads*, position of RNG140. *F*, staining of P0.5 eye slices with anti-RNG140 antibody and DAPI. *Arrowheads*, lens. *Scale bar*, 100 μm. *G*, staining of P0.5 eye slices with WGA and DAPI. *Arrowheads* and *arrows*, lens and lens nucleus, respectively. *Scale bar*, 100 μm. *H*, quantification of lens nucleus diameter normalized to lens diameter. $Rng140^{+/+}$ mice, $n = 9$; $Rng140^{-/-}$ mice, $n = 8$; *, $p = 0.0377$; *t* test.

grew into adults and were fertile, and used them in the analysis below.

As RNG140 is highly expressed in embryonic and postnatal eye lens in mice and RNG140 deficiency causes developmental defect in lens (20), we checked the expression level of RNG140 in the eye of *Rng140*$^{-/-}$ mice at postnatal day 0.5 (P0.5). Quantitative RT-PCR (qRT-PCR) showed that RNG140 transcripts were markedly decreased in the eye of *Rng140*$^{-/-}$ mice, as expected (Fig. 5*D*). Western blotting analysis showed that RNG140 protein was also decreased in the eye of *Rng140*$^{-/-}$ mice (Fig. 5*E*). Immunostaining of eye slices with the anti-RNG140 antibody revealed a decrease in lens fiber cell staining in *Rng140*$^{-/-}$ mice (Fig. 5*F*). We noted that the antibody we raised may also recognize other nonspecific proteins, because high staining intensity outside of the lens was indistinguishable between *Rng140*$^{-/-}$ mice and *Rng140*$^{+/+}$ mice and many bands detected in Western blotting. Together, these results indicated that RNG140 expression was decreased in the eye lens of *Rng140*$^{-/-}$ mice.

The effect of RNG140 knockout on lens development was analyzed by staining of eye slices with wheat germ agglutinin (WGA), which stains lens nucleus regions with less intensity compared with high-intensity staining of lens cortex regions (20). Measuring the diameter of the nucleus region compared with the entire lens region revealed that *Rng140*$^{-/-}$ mice had a significantly reduced size of the lens nucleus compared with *Rng140*$^{+/+}$ mice (Fig. 5, *G* and *H*). These results were consistent with the previous report that RNG140 (caprin2) deficiency showed a defect in lens fiber cell nuclear compaction and reduced the size of the lens nucleus (20).

In vivo relevance of RNG140-mediated translational repression in mouse eyes

Next, we conducted ribosome profiling of *Rng140*$^{-/-}$ mouse eyes at P0.5 and compared it with that of *Rng140*$^{+/+}$ mice (Fig. 6 (*A–D*) and Table S7). For technical feasibility, we isolated whole eyes instead of lenses. This may underestimate differences in translation efficiency between the genotypes, due to non-lens tissues that express low levels of RNG140 and may be less sensitive to RNG140 knockout. However, even underestimated, the results were expected to reflect the impact of RNG140 knockout on the lens. If RNG140-mediated translational repression operates *in vivo*, the effect of RNG140 knockout on translation efficiency is expected to be opposite to that of RNG140 overexpression in CHO cells. Indeed, RNG140 deficiency significantly increased the translation efficiency of the transcripts corresponding to the more-T group in the CHO ribosome profiling but, in contrast, decreased that of the less-T group (Fig. 6*B*). We further examined transcripts that were enriched in the major GO categories in the CHO ribosome profiling: more-T enriched in "HECT" and "PI3K/PI4K" and less-T enriched in "Histone core" and "Ribosomal protein" (Fig. 6*C* and Table S8). Changes in the translation efficiency of these mRNAs in the eyes of RNG140 knockout mice were opposite to those of RNG140 overexpression in CHO cells. These results suggested that the targets of RNG140 were similar between CHO cells and mouse eyes and that changes in translation efficiency correlated with RNG140 dose.

RNG140 was highly expressed during lens differentiation; therefore, a question was raised whether key factors that regulate lens differentiation escape RNG140-mediated translational repression. We thus examined transcripts encoding lens differentiation factors such as α-, β-, and γ-crystallins, lens major intrinsic protein (MIP), CP115, and CP49 (34) (Fig. 6*D* and Table S8). Translation efficiency of these transcripts was reduced by RNG140 deficiency, suggesting that the loss of RNG140 had an effect on global translation, which reduced the relative translation of lens differentiation–related transcripts compared with transcripts that RNG140 would normally repress.

The correspondence between the short CDS in crystallin mRNAs and the length-dependent effect of RNG140 found in CHO cells led us to hypothesize that shortness is the basis for escaping translational repression by RNG140. In fact, in differentiating lenses, shorter CDSs and fewer coding exons were found in translationally decreased transcripts by RNG140 deficiency (Fig. 6*E* and Tables S9 and S10). Taken together, these results suggested that RNG140-mediated translational repression operates in mouse eyes *in vivo*, which reduces the translation of a set of mRNAs, whereas it allows other mRNAs, including those associated with lens differentiation, to escape repression and be translated during lens differentiation.

Discussion

In this study, we characterized RNG140-mediated translational regulation. Several lines of evidence revealed that RNG140 inhibits translation through mechanisms including suppression of eIF3-dependent translation initiation. RNG140 preferentially inhibited the translation of long mRNAs, which can be a way to regulate a specific set of mRNAs. Taken together with the fact that fibroblast growth factor activity drives both RNG140 expression and cell cycle exit during lens differentiation (15, 21), we argue that RNG140 selectively inhibits the translation of long mRNAs involved in cell proliferation, leaving the short mRNAs involved in lens differentiation translated. This mRNA-selective mechanism is likely to underlie the reduction in the size of the lens nucleus, which may be caused by impaired cell cycle exit and delayed lens differentiation by RNG140 (caprin2) deficiency in mouse eyes (20).

A possible mechanism underlying the long mRNA selectivity is that RNG140 binds preferentially to long mRNAs and inhibits their translation through mechanisms such as binding with eIF3. However, the mechanism by which RNG140 prefers long mRNAs remains unclear, except for the hypothesis that the low sequence selectivity of RNG140 increases stochastic interactions with longer mRNAs. Longer mRNAs stretch out long strands in crowded spaces within the cell. In addition, due to the low sequence specificity of RNG140, longer mRNAs provide multiple binding sites for RNG140. Thus, the entire length of the long mRNA may behave like a large antenna, increasing the probability of receiving RNG140 in the crowded space of the cell. Once RNG140 binds to an mRNA, the RNG140-eIF3-ribosome-mRNA complex may be more easily formed in a *cis*-acting than a *trans*-acting manner. This mechanism may not preclude another possibility, that the selectivity depends on the properties of eIF3, as discussed below.

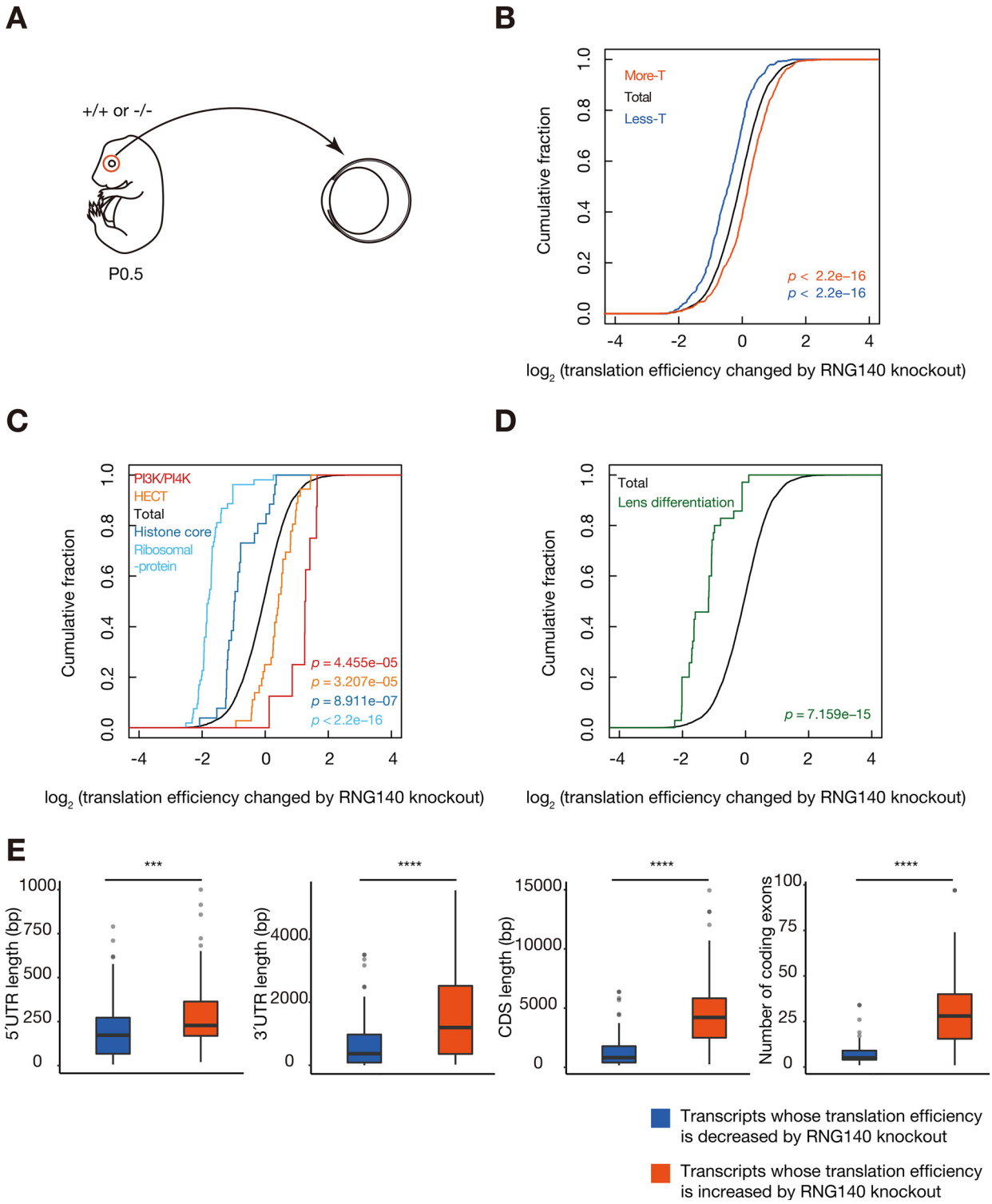

Figure 6. RNG140 deficiency in mouse eyes has an effect on translation efficiency that is opposite to the effect of RNG140 overexpression in CHO cells. *A*, mouse eyes were isolated from P0.5 *Rng140*$^{+/+}$ and *Rng140*$^{-/-}$ mice and subjected to ribosome profiling. *B–D*, cumulative distribution fraction plots showing changes in translation efficiency of transcripts in the indicated groups by RNG140 knockout. Significance is calculated by Mann–Whitney *U* test. *B*, total transcripts and transcripts corresponding to those in the more-T and less-T groups in the CHO ribosome profiling are plotted. *C*, transcripts corresponding to more-T enriched in "HECT" and "PI3K/PI4K" and less-T enriched in "Histone core" and "Ribosomal protein" in the CHO ribosome profiling are plotted. See Table S8 for the transcripts included in each group. *D*, transcripts encoding lens differentiation–related proteins, α-, β-, and γ-crystallins (*Crya*, *Cryb*, and *Cryg*), lens major intrinsic protein (*Mip*), CP115 (*Bfsp1*), and CP49 (*Bfsp2*) are plotted. See Table S8 for the transcripts included. *E*, the top 100 transcripts of which translation efficiency was decreased and increased by RNG140 knockout were analyzed for 5′-UTR length, 3′-UTR length, CDS length, and the number of coding exons. ***, $p = 0.00373$ for 5′-UTR length; ****, $p = 6.79e{-}6$ (for 3′-UTR length), 0.000211 (for CDS length), and $1.61e{-}8$ (for the number of coding exons).

eIF3 is the largest and most complicated translation initiation factor, composed of 13 subunits, and it binds to the eIF4F complex and promotes m^7G cap-dependent translation (35). Besides this general role in translation initiation, eIF3 has been reported to alternatively regulate protein synthesis in a selective and mRNA-specific manner. For example, eIF3 specifically associates with mRNAs such as c-Jun and BTG1 and regulates cell growth in human 293T cells (36). In yeast, eIF3e and eIF3d up-regulate the translation for mitochondrial electron transport chains and ribosome biogenesis (37). In mice, eIF3 is involved in terminal erythroid differentiation by binding to cytoplasmic polyadenylation element–binding protein 4 (CPEB4) and suppressing translation of a set of mRNAs (38). In addition, in zebrafish, eIF3h is required for the translation of certain mRNAs, including crystallin mRNAs, for brain and eye development (19). These studies suggested that eIF3 selectively up-regulates the translation of mRNAs for mitochondrial function, ribosome function, and eye differentiation.

These functional categories are reminiscent of RNG140 non-targeted short mRNAs, which led to the idea that the selective mode of eIF3 works on relatively short mRNAs. In that case, if RNG140 inhibits only the general mode and not the selective mode of eIF3, short mRNAs could selectively escape translational repression by RNG140. In the eIF3h-deficient zebrafish, transcripts that are selectively translated through an eIF3h-dependent mechanism were identified (19). Of these, 19 transcripts corresponded to the orthologs analyzed in the mouse eye in the current study (*Atp2a1*, *Capn3*, *Col15a1*, *Cox4i1*, *Cox6b1*, *Cryba1*, *Cryba2*, *Crybb1*, *Crygn*, *Dusp26*, *Emc4*, *Lim2*, *Mip*, *Mylpf*, *Nefm*, *Pkm*, *Slc25A4*, *Tnnt3*, and *Tyrp1*). The average change in translation efficiency of these 19 transcripts by RNG140 knockout was -0.31 ± 0.24, suggesting that they tend not to be targeted by RNG140. They included the lens differentiation–related transcripts (*Cryba1*, *Cryba2*, *Crybb1*, *Crygn*, and *Mip*), all of which escaped translational repression by RNG140. These results supported the notion that RNG140 has a lesser effect on the selective mode of eIF3. Thus, another possible mechanism is that RNG140 exerts mRNA selectivity through regulating eIF3. Alternatively, RNG140 could specifically up-regulate the selective mode of eIF3. However, the expression levels of lens proteins such as γ-crystallin and lens MIP/Aqp0 were not altered by RNG140 (caprin2) knockout (20), which may support the explanation that RNG140 suppresses the general mode of eIF3.

RNG140 has been reported to form RNA granules that are rich in neither ribosomes nor G3BP (10). Cells containing such granules stop cell division and are more susceptible to cell death than those expressing lower levels of RNG140 without granule formation (10). The CHO cell clones used in the current study did not form granules, and RNG140 interacted with G3BP and ribosomes in these cells. Together, these suggest that at low concentrations, RNG140 binds to G3BP and ribosomes without forming granules, whereas above the critical concentration, RNG140 undergoes phase separation/transition to form granules and rearrange its binding partners.

The granule formation of RNG140 is stage-specific during mouse eye development: RNG140 forms granular structures in lens pit cells at embryonic day 10.5 (E10.5), when the lens vesicle detaches from the surface ectoderm. Later, RNG140 granules disappear, and RNG140 is abundantly expressed without forming granules in lens fiber cells from E12.5 to P4 (20). Thus, RNG140 granules are not static but rather dynamic, by switching condensation-dissolution states at various stages of lens development. It is not known whether the switching is regulated by the expression level of RNG140 or by other mechanisms, such as post-translational modifications of RNG140 granule components in the lens cell. In either case, CHO cells expressing RNG140-GFP used in the current study may resemble the physiological state of lens fiber cells in that they did not contain RNG140 granule structures.

In summary, this study characterized RNG140-mediated translational regulation, providing a mechanistic insight into post-transcriptional regulation that down-regulates proliferation-related factors without suppressing differentiation-related factors during lens development. This study also raised new questions about why and how mRNA length is distinguished by translational regulators in the coordination of proliferation and differentiation. We hope that future research will resolve this question and, in addition, whether this question is limited to lens development or is common to other aspects of cell fate determination and function.

Experimental procedures

Ethics statement

All animal care and experiments were approved by the institutional animal care and use committee of the National Institutes of Natural Sciences and performed in accordance with the guidelines from the National Institutes of Natural Sciences.

Cell culture and transfection

CHO-K1 cells (RCB0285, RIKEN BRC, Tsukuba, Japan) were cultured in Ham's F-12 medium (FUJIFILM Wako Pure Chemical Corp., Osaka, Japan) containing 5% fetal bovine serum (FBS). SRA 01/04 cells (RCB1591, RIKEN BRC) were cultured in low-glucose Dulbecco's modified Eagle's medium (FUJIFILM Wako Pure Chemical Corporation) containing 20% FBS. Cells were placed at 37 °C in a 5% CO_2 incubator. For transfection, cells were grown to ~90% confluence and transfected with plasmids using Lipofectamine 2000 (Thermo Fisher Scientific, Waltham, MA, USA) in accordance with the manufacturer's protocol. Stable transfectants were selected in the presence of 1 mg/ml Geneticin (Thermo Fisher Scientific) in the medium and then obtained by picking up fluorescent colonies with the use of a CKX41 microscope equipped with an epifluorescence module (Olympus, Tokyo, Japan).

Plasmid construction

Plasmids for the expression of RNG140 tagged with GFP and glutathione *S*-transferase (GST) were constructed previously (10). To construct a plasmid for the expression of RNG140 untagged with GFP, a portion of RNG140 CDS was amplified by PCR using primers 5′-CTGTTCTAGATTTTGACAAACCC-3′ and 5′- GGGGGTACCTTAATCTTGATAAAGAAGATAGCCTGAAA-3′, which introduced a stop codon at the 3′ end of the RNG140 CDS. The fragment was cloned into the

XbaI/KpnI sites of the RNG140-GFP plasmid. To construct a control plasmid for the RNG140 expression plasmid, GFP CDS was deleted from pEGFP-N1 (Clontech, Mountain View, CA, USA) with Bsp120I/NotI, and the vector was self-ligated.

To construct plasmids for luciferase reporter assays, DNA fragments of EIF2S3 5′ UTR, HCV IRES, and CrPV IRES were inserted between the T7 promoter and ORF of *Renilla* luciferase (hRluc) in psiCHECK2 vector (Promega, Madison, WI, USA). Plasmids containing EIF2S3 5′-UTR and HCV IRES were constructed previously (24). To construct the plasmid containing the CrPV IRES, the following sequence was inserted: AAAGCAAAAATGTGATCTTGCTTGTAAATACAATTTT-GAGAGGTTAATAAATTACAAGTAGTGCTATTTTTGTA-TTTAGGTTAGCTATTTAGCTTTACGTTCCAGGATGCC-TAGTGGCAGCCCCACAATATCCAGGAAGCCCTCTCTG-CGGTTTTTCAGATTAGGTAGTCGAAAAACCTAAGAAA-TTTACCTGCTACATTTCAAGATA.

To construct a plasmid for Cas9 mRNA preparation, the hCas9 gene was excised with AgeI/EcoRI from pX330 vector (Addgene, Watertown, MA, USA). The fragment was inserted downstream of the SP6 promoter in the pSP64 vector (Promega) and used for *in vitro* transcription. To clone RNG140 guide RNA (gRNA), a pair of oligonucleotides targeting the *Rng140* gene (5′-TAGGGGAAGGTAGTGAAAAAACAG-3′ and 5′-AAACCTGTTTTTTCACTACCTTCC-3′) was annealed and inserted into the BsaI site of the pDR274 vector (Addgene).

Ribopuromycilation assay

The ribopuromycilation assay was performed as described previously (39). Briefly, cells were pulse-labeled with 50 μg/ml puromycin in medium containing 100 μg/ml cycloheximide for 10 min at 37 °C and washed with PBS (137 mM NaCl, 8.1 mM Na_2HPO_4, 1.5 mM KH_2PO_4, and 2.7 mM KCl, pH 7.4) containing 100 μg/ml cycloheximide for 3 min on ice. The cells were permeabilized and fixed with 50 mM Tris-HCl (pH 7.5), 5 mM $MgCl_2$, 25 mM KCl, 100 μg/ml cycloheximide, 0.015% digitonin, and 3.7% formaldehyde for 5 min on ice. After post-fixation with 3.7% formaldehyde in PBS for 10 min at room temperature, the cells were immunofluorescence-stained with an anti-puromycin antibody (3RH11, KeraFAST Inc., Boston, MA, USA) and cyanine 3–conjugated anti-mouse IgG (Jackson ImmunoResearch, West Grove, PA, USA). Cycloheximide was included in the buffers to maintain the association of puromycin-labeled nascent polypeptides with ribosomes, which prevents the labeled polypeptides from being lost from the cells during the permeabilization process with digitonin and enables the detection of translation sites at the subcellular level.

To compare the fluorescence intensity of puromycin staining between GFP-expressing cells and RNG140-GFP–expressing cells, they were co-cultured on the same coverslips. GFP-expressing cells and RNG140-GFP–expressing cells were clearly distinguished by the predominant localization of GFP fluorescence in the nucleus and cytoplasm, respectively. Fluorescence images were acquired using an A1 confocal laser microscope equipped with a Ti-E inverted microscope (Nikon, Tokyo, Japan) with a PlanApo VC60× water objective. For transient transfectants, the average fluorescence intensity of GFP and puromycin staining in the whole-cell area was measured using Fiji software. In the case of stable transfectants, because the cell morphology of each clone was different, total fluorescence intensity (mean fluorescence intensity × cell area) of puromycin staining in the whole-cell area was measured.

Western blotting SUnSET

Puromycin incorporation into nascent polypeptides was quantitatively analyzed by Western blotting SUnSET with modifications to the ribopuromycilation assay. Briefly, cells were pulse-labeled with 20 μM puromycin in cycloheximide-free medium for 30 min at 37 °C. Cells were washed with ice-cold PBS and lysed with 20 mM Tris-HCl, pH 7.5, 150 mM NaCl, 5 mM $MgCl_2$, and 1% Triton X-100. After centrifugation at 20,000 × g for 10 min at 4 °C, the supernatant was subjected to Western blotting with the anti-puromycin antibody (KeraFAST Inc.). The total band intensity of puromycin was normalized with tubulin band intensity probed with anti-α-tubulin antibody (T9026, Sigma–Aldrich). Quantification of band intensity was performed as described previously using a standard curve generated from a standard dilution series of cell extracts on the same membrane (40).

Sucrose density gradient centrifugation

Cells were incubated with 100 μg/ml cycloheximide in the medium for 15 min, washed with ice-cold PBS, and lysed with cell lysis buffer (20 mM Hepes-KOH, pH 7.4, 15 mM $MgCl_2$, 200 mM KCl, 1% Triton X-100, 100 μg/ml cycloheximide, 2 mM DTT, 1 mg/ml heparin, 10 μg/ml leupeptin, 10 μg/ml pepstatin, and 1 mM phenylmethylsulfonyl fluoride). After centrifugation at 14,000 × *g* for 5 min at 4 °C, the supernatant was overlaid onto a 15–45% (w/w) linear sucrose density gradient in cell lysis buffer lacking Triton X-100 and heparin, which had been prepared using a gradient gel–making device (ATTO, Tokyo, Japan), and then centrifuged at 100,000 × *g* for 4 h at 4 °C in an SW41Ti swing rotor (Beckman Coulter, Brea, CA, USA). In experiments without cycloheximide, the drug was removed during the procedures. In EDTA-adding experiments, 0.1 M EDTA was added to the cell lysis buffer and the sucrose density gradient, omitting cycloheximide. After centrifugation, cell lysates remaining on the top of the sucrose gradient were removed, and then the sucrose gradient was fractionated into 22 fractions. RNA was isolated from each fraction using ISOGEN (Nippon Gene, Tokyo, Japan), and the absorbance was measured at 254 nm using NanoDrop (Thermo Fisher Scientific). The relative amount of RNA in each fraction was calculated so that the total amount of RNA in the 22 fractions was 1.00. Sedimentation profiles of 40S, 60S, and 80S ribosomes and polysomes were analyzed by denaturing agarose gel electrophoresis to detect 18S and 28S rRNA.

Ribosome pelleting through a sucrose cushion

Ribosome pellets were prepared as described previously (22). Briefly, cells were incubated with 100 μg/ml cycloheximide in the medium for 15 min, washed with ice-cold PBS, and then lysed with polysome lysis buffer (10 mM Hepes-KOH, pH 7.4, 5 mM $MgCl_2$, 100 mM KCl, 2% Triton X-100, and 100 μg/ml

cycloheximide). After centrifugation at 14,000 × *g* for 10 min at 4 °C, 300 μl of lysate was overlaid onto 900 μl of a 1 M sucrose cushion and centrifuged at 78,000 rpm for 120 min at 4 °C in a TLA-110 rotor (Beckman Coulter). After removing the supernatant, ribosome pellets were rinsed once with polysome lysis buffer and resuspended in Laemmli sample buffer for Western blotting. It should be noted that the ratio of the number of cells to the volume of the lysis buffer was the same between GFP– and RNG140-GFP–expressing clones (5.0×10^6 cells/ml) and that the volume of Laemmli sample buffer added to the ribosome pellets and the volume of lysates and pellets loaded on the SDS-polyacrylamide gel were the same between the clones.

Generation of a polyclonal antibody against RNG140

RNG140 tagged with GST (10) was expressed in *Escherichia coli* (BL21) and purified using GSH-Sepharose 4B columns (GE Healthcare). The GST tag was removed by factor Xa cleavage, and the RNG140 protein was purified in accordance with the manufacturer's protocol. The purified protein was used as an antigen to generate a polyclonal antibody in a rabbit. An anti-RNG140 antibody was affinity-purified from rabbit serum using Affi-Gel 10 gel (Bio-Rad) conjugated with purified RNG140.

Western blotting

Western blotting was performed on polyvinylidene difluoride membranes using the following primary antibodies: anti-RNG140 polyclonal antibody, anti-GFP antibody (GF200, Nacalai Tesque, Kyoto, Japan), anti-eIF3b antibodies (sc-163777 and sc-137214, Santa Cruz Biotechnology, Inc., Dallas, TX, USA), anti-eIF3e antibody (A302-985A, Bethyl Laboratories, Montgomery, TX, USA), anti-eIF3k antibody (NB100-93304, Novus Biologicals, Centennial, CO, USA), anti-eIF3l antibody (GTX120119, GeneTex, Irvine, CA, USA), anti-eEF2 antibody (catalog no. 2332, Cell Signaling Technology, Danvers, MA, USA), anti-S6 ribosomal protein antibody (catalog no. 2317, Cell Signaling Technology), anti-ATR antibody (catalog no. 2790, Cell Signaling Technology), anti-POLA antibody (ab31777, Abcam, Cambridge, UK), anti-RPS18 antibody (ab91293, Abcam), and anti-FBL antibody (ab4566, Abcam). Biotinylated secondary antibodies (GE Healthcare) and alkaline phosphatase–conjugated streptavidin (GE Healthcare) were used to detect the reacted proteins with a solution with bromochloroindolyl phosphate and nitro blue tetrazolium. Quantification of band intensity was performed as described previously using a standard curve generated from a standard dilution series of cell extracts on the same membrane (40).

Immunoprecipitation

Immunoprecipitation was performed as described previously (41). Cells were homogenized in 0.25 M sucrose, 0.7% Triton X-100, 0.1 mM DTT, protease inhibitors (10 μg/ml leupeptin, 10 μg/ml pepstatin, 10 μg/ml aprotinin, and 1 mM phenylmethylsulfonyl fluoride), and 1,000 units/ml RNase inhibitor (Takara Bio, Shiga, Japan) and then centrifuged at 10,000 × *g* for 10 min at 4 °C. The lysate was added to a 1:10 volume of 10× PBS followed by a 1:20 volume of anti-GFP-agarose beads (Medical and Biological Laboratories, Nagoya, Japan). After rocking for 2 h at 4 °C, the beads were washed three times with PBS containing 0.1 mM DTT, the protease inhibitors, and 100 units/ml RNase inhibitor. For RNase treatment, 0.2 mg/ml RNase A (FUJIFILM Wako Pure Chemical Corp.) was added, omitting RNase inhibitor in the lysis buffer and the wash buffer. It should be noted that the ratio of the number of cells to the volume of homogenization buffer was the same between GFP– and RNG140-GFP–expressing clones (6.0×10^6 cells/ml) and that the volume of cell lysates and volume of beads loaded on the SDS-polyacrylamide gel were the same between the clones.

MS

Proteins in immunoprecipitates with the anti-GFP antibody were separated by SDS-PAGE and stained with Coomassie Brilliant Blue. Gel slices with corresponding protein bands were excised and then destained with 30% acetonitrile in 25 mM NH_4HCO_3 for 10 min. The gel slices were dehydrated with 50% acetonitrile in 25 mM NH_4HCO_3 for 10 min and dried in a vacuum desiccator. After rehydrating the gel slices with 10 μg/ml trypsin in 50 mM NH_4HCO_3 for 30 min on ice, excess solution was removed, and the gel slices were incubated for 12 h at 37 °C for in-gel digestion. Digested peptides were extracted with 50% acetonitrile and 5% CF_3COOH for 1 h at room temperature and then analyzed with an Orbitrap Elite mass spectrometer (Thermo Fisher Scientific). The peptides were eluted using a 20-min acetonitrile gradient (10-min 0–30% acetonitrile gradient, followed by a 2-min 30–80% gradient, with a final 8-min isocratic step at 80% acetonitrile) at a flow rate of 300 nl/min. Singly charged ions (and unassigned charge states) were excluded.

Peak lists were generated from raw data using Proteome Discoverer 2.2 software (Thermo Fisher Scientific). The peak list files were searched against the NCBIprot (20200204; 257,100,649 sequences) (National Center for Biotechnology Information, Bethesda, MD, USA) using Mascot software (version 2.6.1) (Matrix Science, London, UK). Trypsin was selected as the enzyme, with two potential missed cleavages. Fragment ion mass tolerance was set to 0.8 Da, and precursor ion mass tolerance was set to 10 ppm. Variable amino acid modification was oxidized methionine, and there was no fixed amino acid modification. Peptide spectral matches were filtered to a 1% false discovery rate using the target-decoy strategy combined with linear discriminant analysis. Proteins with only a single peptide identified were removed from the list. If proteins were contained in the control GFP immunoprecipitates in an amount comparable with those in the RNG140-GFP immunoprecipitates, as judged by the Mascot score ratio of the protein in the RNG140-GFP immunoprecipitates to the GFP immunoprecipitates being less than 2.5, those proteins were also removed from the list.

Two biological replicates were acquired. One was a pilot experiment, and the other was a large-scale experiment. The results acquired from the latter are shown as Table S1 and have been deposited in the PRIDE repository. The results of the two experiments were reproducible except that the pilot

experiment detected only major proteins, including eIF3 subunits and ribosomal small subunit proteins.

Translation reporter assay

Stable cell lines of GFP and RNG140-GFP were transfected with plasmids encoding CrPV IRES-hRluc, HCV IRES-hRluc, or EIF2S3 5′-UTR-hRluc in 96-well dishes. hRluc luciferase assays were performed using the Renilla-Glo Luciferase Assay System (Promega) in accordance with the manufacturer's protocol. The luminescence was quantified using a Corona SH-9000Lab (HITACHI, Tokyo, Japan) and normalized by the amount of the hRluc transcripts measured by qRT-PCR as described below.

Quantitative RT-PCR

Total RNA was extracted from cell lysates or mouse tissues using ISOGEN (Nippon Gene) in accordance with the manufacturer's protocol. RT was performed with M-MLV-Reverse Transcriptase (Thermo Fisher Scientific), and quantitative PCR was performed with SYBR Premix Ex Taq II (Tli RNaseH Plus) (Takara Bio) using a 7500 real-time PCR system (Applied Biosystems, Carlsbad, CA, USA) in accordance with the manufacturer's protocol. The primers used for qPCR were as follows: hRluc, 5′-ACGCAAACGCATGATCACTG-3′ and 5′-GCAGAAAAATCACGGCGTTC-3′; GAPDH, 5′-AACGACCCCTTCATTGACCT-3′ and 5′-TGGAAGATGGTGATGGGCTT-3′; RNG140, 5′-AGAGCAGCTTAACCCAGACCAGTTG-3′ and 5′-GGGCCTTTTTCTGCGCTTTCAGC-3′.

Ribosome profiling and RNA-Seq

Ribosome profiling was performed as reported previously (42) with modifications. Cultured CHO cells or eyes excised from P0.5 mice were washed with ice-cold PBS, lysed with ice-cold lysis buffer (20 mM Tris-HCl, pH 7.5, 150 mM NaCl, 5 mM $MgCl_2$, 1 mM DTT, 100 μg/ml cycloheximide, and 1% Triton X-100), treated with TURBO DNase (25 units/ml at final concentration, Thermo Fisher Scientific), and centrifuged at 20,000 × *g* for 10 min at 4 °C. For eyes, bead shocker (Yasui Kikai, Osaka, Japan) was used for lysis. The RNA concentration of this lysate was measured using a Qubit RNA HS Assay Kit (Thermo Fisher Scientific). CHO cell lysate containing 10 μg of RNA and mouse eye lysate containing 3 μg of RNA were treated with 20 and 6 units of RNase I (Lucigen, Middleton, WI, USA) at 25 °C for 45 min. The sample was overlaid on a 1 M sucrose cushion, and the ribosomes were pelleted by centrifugation for 1 h at 100,000 rpm at 4 °C in a TLA-110 rotor. Ribosome-bound RNA was isolated using a Direct-zol RNA MicroPrep kit (Zymo Research, Irvine, CA, USA). After gel electrophoresis, RNA fragments corresponding to 26–34 nt were excised and subjected to library construction as described previously (42).

RNA-Seq analysis was performed on total RNA extracted from the exact same lysate used for ribosome profiling, using TRIzol reagent (Thermo Fisher Scientific). rRNAs were removed from the total RNA using the Ribo-Zero Gold rRNA Removal Kit (Human/Mouse/Rat) (Illumina, San Diego, CA, USA), and cDNA libraries were prepared using the TruSeq Stranded mRNA Library Prep Kit (Illumina).

The libraries were sequenced on a HiSeq4000 (Illumina), and the reads were aligned to the Chinese hamster genome (criGri1) and the mouse genome (GRCm38/mm10). For ribosome profiling, the offsets of the A-site from the 5′ end of ribosome footprints were determined to be 12 for 25 nt, 13 for 26 nt, 14 for 27 nt, 15 for 28 nt, and 16 for 29–30 nt in cultured CHO cells and 15 for 26–29 nt and 16 for 30–31 nt in mouse eyes. For RNA-Seq analysis, offset 15 was used for all mRNA fragments. To count the number of footprints in the CDS, footprints corresponding to the first and last five codons of the CDS were excluded. To calculate the translation efficiency, ribosome profiling counts were normalized by RNA-Seq counts using the DESeq package (43). Two and three independent experiments were conducted for CHO cells and mouse eyes, respectively, and the data were analyzed statistically. All custom scripts used in this study are available upon request.

Gene ontology analysis

GO enrichment analysis was performed using PANTHER gene list analysis tools and DAVID functional annotation tools. Significance of overrepresentation of GO terms was assessed using the Benjamini–Hochberg false discovery rate criterion at $q < 0.05$.

Transcript length and exon numbers

The length of UTR and CDS and the number of coding exons of transcripts were obtained from Ensembl database.

Cell proliferation assay

CHO cells stably expressing RNG140-GFP or GFP were seeded in 6-well cell culture plates (1×10^4 cells/well) and incubated at 37 °C with 5% CO_2. After washing with saline, the cells were detached from the plate with 0.25% trypsin-EDTA (Thermo Fisher Scientific) and counted using a hemocytometer. Cells were counted daily for 5 days after seeding.

Preparation of Cas9 mRNA and gRNA

The spSP64-hCas9 plasmid was linearized by digestion with SalI and used for *hCas9* mRNA preparation by an mMESSAGE mMACHINE SP6 transcription kit (Thermo Fisher Scientific) in accordance with the manufacturer's protocol. For RNG140 gRNA preparation, the plasmids were digested with DraI and used for *in vitro* transcription by a MEGAshortscript T7 transcription kit (Thermo Fisher Scientific). The synthesized mRNA and gRNA were purified using phenol-chloroform-isoamyl alcohol extraction and isopropyl alcohol precipitation. The precipitated RNA was dissolved in Opti-MEM I (Thermo Fisher Scientific) at 2–4 μg/μl.

Generation of RNG140 knockout mice

RNG140 knockout mice were generated using a CRISPR/Cas9 system with modifications to a previous report (44). *In vitro* fertilized eggs from C57BL/6J strain mice were cultured in modified Whitten's medium (mWM) for 2 h, washed three times with Opti-MEM I, and then aligned in an electrode gap

(LF501PT1-10, BEX, Tokyo, Japan), which had been filled with 5 μl of Opti-MEM I containing 750 ng/μl Cas9 mRNA and 400 ng/μl gRNA. Electroporation was performed using an SEN-3401 electronic stimulator (NIHON KOHDEN, Tokyo, Japan) with 35 V (3 ms ON + 97 ms OFF) six times, changing the current direction alternately. After electroporation, the eggs were washed four times with M2 medium and two times with mWM and cultured in mWM at 37 °C in a 5% CO_2 incubator. On the next day, surviving two-cell stage zygotes were transferred to the oviducts of pseudopregnant females.

To analyze CRISPR/Cas9-mediated mutations in the *Rng140* gene, the genome region flanking the gRNA target was amplified by PCR using primers 5′-TTCCTTTTCACTTCAGTTGGTTTAG-3′ (RNG140-F1) and 5′-ATGTAAGTTCTGATGGACTGACACA-3′, and then sequenced using the RNG140-F1 primer. For genotyping of WT mice and the 5-bp deleted RNG140 knockout mice, primers RNG140-F1 and 5′-CTCACATGTTGTTCCTACCACTG-3′ were used to detect the WT allele and primers RNG140-F1 and 5′- CACATGTTGTTCCTACTTTTTTC-3′ were used to detect the RNG140 knockout allele.

Immunofluorescence and WGA staining

To stain sections of mouse eyes, P0.5 mouse heads were embedded in Tissue-Tek (Sakura Finetek, Tokyo, Japan), frozen in liquid nitrogen, and horizontally sectioned at 12-μm thickness using a cryostat (Leica CM1950, Leica, Wetzlar, Germany). The sections attached to coverslips were fixed with 3.7% formaldehyde in PBS for 10 min at room temperature. After washing with PBS, the specimens were treated with 0.5% Triton X-100 in PBS, washed with PBS, and blocked with 10% FBS. For immunostaining, the specimens were incubated with the anti-RNG140 antibody and then labeled with an Alexa 488–conjugated anti-rabbit IgG antibody (Thermo Fisher Scientific). For WGA staining, they were incubated with WGA conjugated with Alexa 594 (Thermo Fisher Scientific). Fluorescence images were acquired using the A1 confocal laser microscope equipped with a Ti-E inverted microscope (Nikon) with a ×10 objective.

The images from the WGA staining were used to measure the size of the lens nucleus region compared with the entire lens region using Fiji software. From the serial sections of a mouse head, 2–3 sections with the largest lens diameter were selected. WGA fluorescence intensity was measured along the diameter, perpendicular to the cornea, of the lens nucleus region and the entire lens region. To reduce the noise in the fluorescence intensity waveform along the diameter, the fluorescence intensity of a pixel (position X) was converted to the average of 31 adjacent pixels (position $X \pm 15$). The diameter of the entire lens region corresponded to 500–600 pixels. The average of the maximum and minimum fluorescence intensity was calculated and defined as the boundary value between the lens nucleus and the lens cortex: the region with less fluorescence than that value was considered to be the lens nucleus region. The ratio of the diameter of the lens nucleus to that of the entire lens was calculated from 2–3 replicates from three mice for each genotype.

Statistical analysis

Data are represented as box plots or as the mean with dot plots of individual values. Two samples were compared using an unpaired *t* test. Statistical analysis was performed with R. The GO term enrichment was analyzed using PANTHER gene list analysis tools (RRID:SCR_004869) and DAVID functional annotation tools (RRID:SCR_001881).

Data availability

The results of MS of CHO cells have been deposited to ProteomeXchange Consortium via the PRIDE partner repository with the data set identifier PXD019040. The results of ribosome profiling and RNA-Seq of CHO cells (GSE141840) and mouse eyes (GSE141842) used in this study were deposited in the National Center for Biotechnology Information (NCBI) Gene Expression Omnibus (GEO).

Acknowledgments—We thank Dr. M. Hashimoto for advice on generating RNG140 knockout mice using the CRISPR/Cas9 system; S. Ohsawa for the generation of RNG140 knockout mice; Y. Makino for mass spectrometry; M. Mito and C. Matsuda for technical assistance; and the Spectrography and Bioimaging Facility, Functional Genomics Facility, and Model Animal Research Facility of the National Institute for Basic Biology for technical support. This work used the Vincent J. Coates Genomics Sequencing Laboratory at UC Berkeley, supported by National Institutes of Health Instrumentation Grant S10 OD018174.

Author contributions—K. N. and N. S. conceptualization; K. N. investigation; K. N. visualization; K. N. and N. S. writing-original draft; Y. S. and S. I. resources; Y.S. and S. I. methodology; Y. S., S. I., and N. S. writing-review and editing; N. S. supervision; N. S. funding acquisition; N. S. project administration.

Funding and additional information—This work was supported by the Takeda Science Foundation and Grant-in-Aid for Scientific Research 19H03161 from the Japan Society for the Promotion of Science (JSPS) (to N. S.). This work was supported in part by the Graduate University for Advanced Studies, SOKENDAI. S. I. was supported by Grant-in-Aid for Scientific Research on Innovative Areas "nascent chain biology" JP17H05679, Grant-in-Aid for Young Scientists (A) JP17H04998, Challenging Research (Exploratory) Grant JP19K22406 from JSPS, Pioneering Projects ("Cellular Evolution") and the Aging Project from RIKEN, and the Takeda Science Foundation. Y. S. received JSPS Research Fellowship (PD) 19J00920.

Conflict of interest—The authors declare that they have no conflicts of interest with the contents of this article.

Abbreviations—The abbreviations used are: RNG, RNA granule protein; CHO, Chinese hamster ovary; eIF, eukaryotic initiation factor; eEF, eukaryotic elongation factor; IRES, internal ribosome entry site; more-T, more likely target transcripts; less-T, less likely target transcripts; CDS, coding sequence; GO, gene ontology; PI3K, phosphoinositide 3-kinase; PI4K, phosphoinositide 4-kinase; P, postnatal day; E, embryonic day; qRT-PCR, quantitative RT-PCR; WGA, wheat germ agglutinin; FBS, fetal bovine serum;

GST, glutathione *S*-transferase; gRNA, guide RNA; mWM, modified Whitten's medium; DAPI, 4′,6-diamidino-2-phenylindole; nt, nucleotides.

References

1. Mata, J., Marguerat, S., and Bähler, J. (2005) Post-transcriptional control of gene expression: a genome-wide perspective. *Trends Biochem. Sci.* **30,** 506–514 CrossRef Medline
2. Keene, J. D. (2007) RNA regulons: coordination of post-transcriptional events. *Nat. Rev. Genet.* **8,** 533–543 CrossRef Medline
3. Hieronymus, H., and Silver, P. A. (2004) A systems view of mRNP biology. *Genes Dev.* **18,** 2845–2860 CrossRef Medline
4. Teixeira, F. K., and Lehmann, R. (2019) Translational control during developmental transitions. *Cold Spring Harb. Perspect. Med.* **11,** a032987 CrossRef
5. Tahmasebi, S., Amiri, M., and Sonenberg, N. (2018) Translational control in stem cells. *Front. Genet.* **9,** 709 CrossRef Medline
6. Glisovic, T., Bachorik, J. L., Yong, J., and Dreyfuss, G. (2008) RNA-binding proteins and post-transcriptional gene regulation. *FEBS Lett.* **582,** 1977–1986 CrossRef Medline
7. Kishore, S., Luber, S., and Zavolan, M. (2010) Deciphering the role of RNA-binding proteins in the post-transcriptional control of gene expression. *Brief. Funct. Genomics* **9,** 391–404 CrossRef Medline
8. Ding, Y., Xi, Y., Chen, T., Wang, J. Y., Tao, D. L., Wu, Z. L., Li, Y. P., Li, C., Zeng, R., and Li, L. (2008) Caprin-2 enhances canonical Wnt signaling through regulating LRP5/6 phosphorylation. *J. Cell Biol.* **182,** 865–872 CrossRef Medline
9. Aerbajinai, W., Lee, Y. T., Wojda, U., Barr, V. A., and Miller, J. L. (2004) Cloning and characterization of a gene expressed during terminal differentiation that encodes a novel inhibitor of growth. *J. Biol. Chem.* **279,** 1916–1921 CrossRef Medline
10. Shiina, N., and Tokunaga, M. (2010) RNA granule protein 140 (RNG140), a paralog of RNG105 localized to distinct RNA granules in neuronal dendrites in the adult vertebrate brain. *J. Biol. Chem.* **285,** 24260–24269 CrossRef Medline
11. Konopacka, A., Greenwood, M., Loh, S. Y., Paton, J., and Murphy, D. (2015) RNA binding protein Caprin-2 is a pivotal regulator of the central osmotic defense response. *ELife* **4,** e09656 CrossRef
12. Tang, Y. T., Hu, T., Arterburn, M., Boyle, B., Bright, J. M., Palencia, S., Emtage, P. C., and Funk, W. D. (2005) The complete complement of C1q-domain-containing proteins in *Homo sapiens*. *Genomics* **86,** 100–111 CrossRef Medline
13. Miao, H., Jia, Y., Xie, S., Wang, X., Zhao, J., Chu, Y., Zhou, Z., Shi, Z., Song, X., and Li, L. (2014) Structural insights into the C1q domain of Caprin-2 in canonical Wnt signaling. *J. Biol. Chem.* **289,** 34104–34113 CrossRef Medline
14. Flores, R., and Zhong, G. (2015) The *Chlamydia pneumoniae* inclusion membrane protein Cpn1027 interacts with host cell Wnt signaling pathway regulator cytoplasmic activation/proliferation-associated protein 2 (Caprin2). *PLoS ONE* **10,** e0127909 CrossRef Medline
15. Cvekl, A., and Zhang, X. (2017) Signaling and gene regulatory networks in mammalian lens development. *Trends Genet.* **33,** 677–702 CrossRef Medline
16. Cvekl, A., and Ashery-Padan, R. (2014) The cellular and molecular mechanisms of vertebrate lens development. *Development* **141,** 4432–4447 CrossRef Medline
17. Dash, S., Siddam, A. D., Barnum, C. E., Janga, S. C., and Lachke, S. A. (2016) RNA-binding proteins in eye development and disease: implication of conserved RNA granule components. *Wiley Interdiscip. Rev. RNA* **7,** 527–557 CrossRef Medline
18. Lachke, S. A., Alkuraya, F. S., Kneeland, S. C., Ohn, T., Aboukhalil, A., Howell, G. R., Saadi, I., Cavallesco, R., Yue, Y., Tsai, A. C., Nair, K. S., Cosma, M. I., Smith, R. S., Hodges, E., Alfadhli, S. M., *et al.* (2011) Mutations in the RNA granule component TDRD7 cause cataract and glaucoma. *Science* **331,** 1571–1576 CrossRef Medline
19. Choudhuri, A., Maitra, U., and Evans, T. (2013) Translation initiation factor eIF3h targets specific transcripts to polysomes during embryogenesis. *Proc. Natl. Acad. Sci. U. S. A.* **110,** 9818–9823 CrossRef Medline
20. Dash, S., Dang, C. A., Beebe, D. C., and Lachke, S. A. (2015) Deficiency of the RNA binding protein caprin2 causes lens defects and features of peters anomaly. *Dev. Dyn.* **244,** 1313–1327 CrossRef Medline
21. Lorén, C. E., Schrader, J. W., Ahlgren, U., and Gunhaga, L. (2009) FGF signals induce Caprin2 expression in the vertebrate lens. *Differentiation* **77,** 386–394 CrossRef Medline
22. Liu, B., and Qian, S. B. (2016) Characterizing inactive ribosomes in translational profiling. *Translation* **4,** e1138018 CrossRef Medline
23. Kieft, J. S. (2008) Viral IRES RNA structures and ribosome interactions. *Trends Biochem. Sci.* **33,** 274–283 CrossRef Medline
24. Iwasaki, S., Floor, S. N., and Ingolia, N. T. (2016) Rocaglates convert DEAD-box protein eIF4A into a sequence-selective translational repressor. *Nature* **534,** 558–561 CrossRef Medline
25. Ingolia, N. T. (2016) Ribosome footprint profiling of translation throughout the genome. *Cell* **165,** 22–33 CrossRef Medline
26. Ingolia, N. T., Ghaemmaghami, S., Newman, J. R., and Weissman, J. S. (2009) Genome-wide analysis *in vivo* of translation with nucleotide resolution using ribosome profiling. *Science* **324,** 218–223 CrossRef Medline
27. Shiina, N., Shinkura, K., and Tokunaga, M. (2005) A novel RNA-binding protein in neuronal RNA granules: regulatory machinery for local translation. *J. Neurosci.* **25,** 4420–4434 CrossRef Medline
28. Khong, A., Matheny, T., Jain, S., Mitchell, S. F., Wheeler, J. R., and Parker, R. (2017) The stress granule transcriptome reveals principles of mRNA accumulation in stress granules. *Mol. Cell* **68,** 808–820 CrossRef Medline
29. Mishra, A., Godavarthi, S. K., and Jana, N. R. (2009) UBE3A/E6-AP regulates cell proliferation by promoting proteasomal degradation of p27. *Neurobiol. Dis.* **36,** 26–34 CrossRef Medline
30. Okada, M., Ohtake, F., Nishikawa, H., Wu, W., Saeki, Y., Takana, K., and Ohta, T. (2015) Liganded ERα stimulates the E3 ubiquitin ligase activity of UBE3C to facilitate cell proliferation. *Mol. Endocrinol.* **29,** 1646–1657 CrossRef Medline
31. Li, Y., Zhang, L., Zhou, J., Luo, S., Huang, R., Zhao, C., and Diao, A. (2015) Nedd4 E3 ubiquitin ligase promotes cell proliferation and autophagy. *Cell Prolif.* **48,** 338–347 CrossRef Medline
32. Yu, J. S. L., and Cui, W. (2016) Proliferation, survival and metabolism: the role of PI3K/AKT/mTOR signalling in pluripotency and cell fate determination. *Development* **143,** 3050–3060 CrossRef Medline
33. Herceg, Z., Hulla, W., Gell, D., Cuenin, C., Lleonart, M., Jackson, S., and Wang, Z. Q. (2001) Disruption of Trrap causes early embryonic lethality and defects in cell cycle progression. *Nat. Genet.* **29,** 206–211 CrossRef Medline
34. De Longh, R. U., Lovicu, F. J., Overbeek, P. A., Schneider, M. D., Joya, J., Hardeman, E. D., and McAvoy, J. W. (2001) Requirement for TGFβ receptor signaling during terminal lens fiber differentiation. *Development* **128,** 3995–4010 Medline
35. Valášek, L. S., Zeman, J., Wagner, S., Beznosková, P., Pavlíková, Z., Mohammad, M. P., Hronová, V., Herrmannová, A., Hashem, Y., and Gunišová, S. (2017) Embraced by eIF3: structural and functional insights into the roles of eIF3 across the translation cycle. *Nucleic Acids Res.* **45,** 10948–10968 CrossRef Medline
36. Lee, A. S. Y., Kranzusch, P. J., and Cate, J. H. D. (2015) eIF3 targets cell-proliferation messenger RNAs for translational activation or repression. *Nature* **522,** 111–114 CrossRef Medline
37. Shah, M., Su, D., Scheliga, J. S., Pluskal, T., Boronat, S., Motamedchaboki, K., Campos, A. R., Qi, F., Hidalgo, E., Yanagida, M., and Wolf, D. A. (2016) A transcript-specific eIF3 complex mediates global translational control of energy metabolism. *Cell Rep.* **16,** 1891–1902 CrossRef Medline
38. Hu, W., Yuan, B., and Lodish, H. F. (2014) Cpeb4-mediated translational regulatory circuitry controls terminal erythroid differentiation. *Dev. Cell* **30,** 660–672 CrossRef Medline
39. Shiina, N. (2019) Liquid- and solid-like RNA granules form through specific scaffold proteins and combine into biphasic granules. *J. Biol. Chem.* **294,** 3532–3548 CrossRef Medline

40. Ohashi, R., Takao, K., Miyakawa, T., and Shiina, N. (2016) Comprehensive behavioral analysis of RNG105 (Caprin1) heterozygous mice: reduced social interaction and attenuated response to novelty. *Sci. Rep.* **6,** 20775 CrossRef Medline
41. Shiina, N., and Nakayama, K. (2014) RNA granule assembly and disassembly modulated by nuclear factor associated with double-stranded RNA 2 and nuclear factor 45. *J. Biol. Chem.* **289,** 21163–21180 CrossRef Medline
42. McGlincy, N. J., and Ingolia, N. T. (2017) Transcriptome-wide measurement of translation by ribosome profiling. *Methods* **126,** 112–129 CrossRef Medline
43. Anders, S., and Huber, W. (2010) Differential expression analysis for sequence count data. *Genome Biol.* **11,** R106 CrossRef Medline
44. Hashimoto, M., and Takemoto, T. (2015) Electroporation enables the efficient mRNA delivery into the mouse zygotes and facilitates CRISPR/Cas9-based genome editing. *Sci. Rep.* **5,** 11315 CrossRef Medline